Hindawi
Shock and Vibration
Volume 2024, Article ID 9978340, 15 pages
https://doi.org/10.1155/2024/9978340

Research Article

In-Plane Dynamic Cushioning Performance of Concave Hexagonal Honeycomb Cores

Miao Liu,[1] **Yan Cao**,[1] **De-Qiang Sun**,[2] **Chao-Rui Nie**,[3] **and Zhi-Jie Wang**[4]

[1]*School of Mechatronic Engineering, Xi'an Technological University, Xi'an 710021, China*
[2]*Shaanxi Province Key Laboratory of Papermaking Technology and Specialty Paper, National Demonstration Center for Experimental Light Chemistry Engineering Education, Shaanxi University Science and Technology, Xi'an 710021, China*
[3]*School of Automotive Engineering and General Aviation, Shaanxi Vocational and Technical College, Xi'an 710100, China*
[4]*Inner Mongolia North Heavy Industries Group Corp. LTD, Baotou 014033, China*

Correspondence should be addressed to Miao Liu; 414644849@qq.com

Received 22 March 2023; Revised 30 August 2023; Accepted 13 February 2024; Published 11 March 2024

Academic Editor: Matteo Filippi

In order to further study the cushioning performance of concave hexagonal cores (CHCs) and expand their application range, the in-plane finite element model of CHCs is established in this paper. A dynamic cushioning coefficient method was proposed to characterize the cushioning performance of CHCs. The dynamic cushioning coefficient curve and minimum dynamic cushioning coefficient (MDCC) of CHCs with different impact velocities and structural parameters are obtained. The influence rules of structural parameters and impact velocities on the MDCC are analyzed; the deformation mode and transformation empirical formula are also obtained. The results show that when other parameters are constant, the MDCC of CHCs decreases with the increase of impact velocity, increases with the increase of wall thickness and side length ratio, and decreases with the increase of expansion angle. The theoretical analysis is consistent with the finite element results, which further verifies the reliability of the model. This paper provides a solid theoretical basis for the industrial application of the cushioning performance of CHCs and forms a key technical support.

1. Introduction

Porous solid honeycomb cores are widely used in aerospace, automobile transportation, construction engineering, product packaging, and other fields because of their good cushioning performance when subjected to impact and vibration. The honeycomb structure also has an excellent energy absorption capacity, sound absorption capacity, and heat absorption capacity [1, 2]. Porous solid honeycomb cores can be divided into regular type and irregular type according to different geometric topological structures. Regular-type structures include regular hexagon, triangle, circle, and concave hexagon. Concave hexagonal honeycomb is a typical honeycomb structure, and it is the material with negative Poisson's ratio. Negative Poisson's ratio materials have strong application value; they have good industrial application prospects in engineering biomedicine, aerospace, construction, navigation, and other fields [3–7]. As a typical porous cushioning material with negative Poisson's ratio, concave hexagonal honeycomb cores (CHCs) have many unique advantages and have become one of the indispensable porous cushioning materials. As for cushioning materials, energy absorption performance characterization and cellular structure optimization are currently the research focus of scholars at home and abroad. Accurate characterization of energy absorption and cushioning performance can guide the optimization design of material structure and expand the application field of materials, which is of great significance for CHCs.

Domestic and foreign scholars have carried out a series of studies on CHCs with negative Poisson's ratio structure. Li et al. [8] compared the concave hexagonal honeycomb

structure with the regular quadrilateral and hexagonal honeycomb structures, and the research showed that under the same impact load, the concave hexagonal honeycomb structure has higher compression modulus, yield strength, and surface specific energy absorption, the energy absorption effect is optimal, and the shock wave attenuation characteristics are better than other structures. Li et al. [9] compared the macromechanical responses of four honeycomb structures under quasistatic compression. The results show that the honeycomb structure with negative Poisson's ratio gets extra support due to the shrinkage of the matrix, which enhances the stiffness and energy absorption properties. The abovementioned studies show that CHCs have excellent energy absorption performance, and it is of great significance to further quantify the influence of its structural parameters and impact velocity on the energy absorption performance.

Shen et al. [10, 11] studied and analyzed the dynamic performance of hexagonal honeycomb of aluminum substrate under different impact velocities. On this basis, the dynamic response of CHCs is studied deeply. Zhang et al. [12] studied the dynamic impact crushing behavior of open-cell aluminum foam with negative Poisson's ratio effect through finite element numerical simulation and discussed their platform stress, specific energy absorption, and deformation mode. Hu et al. [13] studied the influence of different concave forms of concave triangular honeycomb on the platform stress, specific energy absorption value, and deformation mode under the action of axial impact through numerical simulation. The result show that the less the number of concave edges, the more obvious the negative Poisson's ratio effect. The structural platform with unilateral internal and internal concave has higher stress, longer stress response time, and better energy absorption effect. Ma et al. [14] compared the platform stress and energy absorption of the concave triangular honeycomb structure with different number of concave edges and angles under impact at different velocities. The results show that the stress and energy absorption of the structure with only concave bottom edge are greater than those of the structure with three concave bottom edge. With the increase of impact velocity, the stress and energy absorption capacity of the concave triangular honeycomb are increased. Zhao et al. [15] used the finite element software ABAQUS to analyze the in-plane impact characteristics and deformation modes of three similar concave hexagonal honeycomb structures at low, medium, and high speed in the concave direction. Alomarah et al. [16] proposed a new structure with a negative Poisson's ratio and its in-plane mechanical properties were improved. The Poisson's ratio of honeycomb can be changed by adjusting the new cylindrical structure. It can be seen from the abovementioned research that the current research on CHCs with negative Poisson ratio mostly focuses on the impact velocity and the number of concave edges on the platform stress and energy absorption. In fact, the cellular structural parameters such as wall thickness, side length, and expansion angle of CHCs can affect their mechanical properties.

It is common for honeycomb core materials to bear loads such as impact and collision in practical applications, so accurate characterization of dynamic cushioning performance is particularly important. For CHCs, there is little research on this aspect. At present, the energy absorption cushioning performance characterization methods mainly include the cushioning curve method, capacity absorption curve method, energy absorption diagram method, Janssen factor method, and Rusch curve method [17]. The cushioning coefficient curve characterization can consider many factors such as force area and thickness. Further introducing dynamic cushioning coefficient can more accurately and truly reflect the cushioning performance of honeycomb materials in practical applications, and it can also overcome the shortcomings of static parameters in characterizing the buffering performance of honeycomb materials.

To sum up, in this paper, based on the finite element numerical analysis method (FEM), the in-plane high-speed crushing process of CHCs is simulated, and aluminum is selected as the matrix material. Through relevant post-processing software, the dynamic cushioning coefficient curve and the minimum dynamic cushioning coefficient of CHCs were obtained based the results of FEM. The influence law of related structural parameters and impact velocities on the minimum cushioning coefficient was analyzed. It provides the theoretical basis for the structure optimization, performance improvement, and further application of CHCs.

2. Model Description

2.1. Finite Element Model. Sun et al. [18] framed the FE model for the in-plane impact of CHCs by following the previous FE investigations about the mechanics of cellular materials. The similar full-scale FE model is used here. The model for in-plane dynamic cushioning analysis is shown in Figure 1. ANSYS/LS-DYNA software is employed here to simulate the in-plane cushioning performance of CHCs along the x_1 direction. The number of cells in the x_1 and x_2 directions are 11 and 15, respectively. The specimen of CHCs is placed between the upper pressing plate (P1) and the support plate (P2), both of which are rigid. The mass of the upper pressing plate is large enough to ensure that the specimens are crushed. When the model is loaded, the support rigid plate (P2) is fixed, and the upper rigid plate (P1) impacts the specimen along the direction x_1 at a constant speed v.

The bottom end of the honeycomb structure is bound to the fixed-end rigid body, and the left and right sides are free in plane. The displacement constraint of the honeycomb structure in the x_3 direction is 0 to ensure that the honeycomb always meets the plane strain state during the impact process. The honeycomb structure was meshed with square Belytschko Shell163 elements with five integration points and an element edge length of 0.3 mm. The entire model defines single face frictionless automatic contact, and the honeycomb body and two rigid plates are defined as surface-to-surface automatic contact, with a friction coefficient of 0.02. The single surface automatic contact is set among the cells in the honeycomb in case the structure penetrates each other during crushing [19].

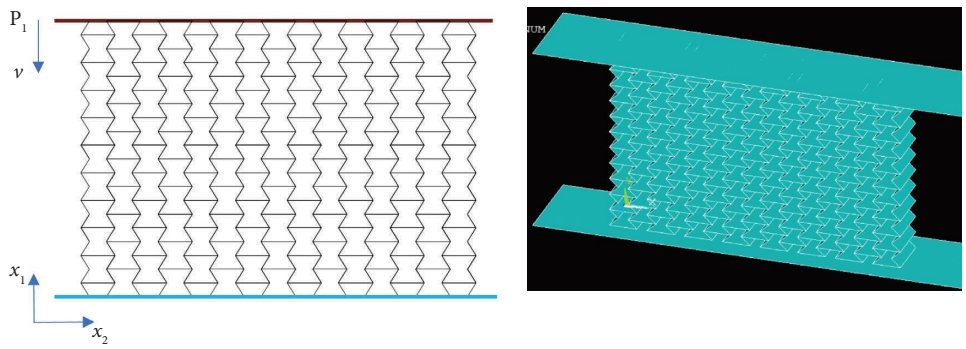

(a) (b)

Figure 1: FE model of concave hexagonal honeycomb cores. (a) Two-dimensional FE model. (b) Three-dimensional FE model.

The impact velocity is shown in Table 1. Following Sun and Zhang [20], the bilinear strain-hardening model (see Figure 2(b)) is used to represent the constitutive relationship of basis material, which is typically aluminum. The mechanical properties of basis material are shown in Table 2. This model is suited for modeling isotropic and kinematic hardening plasticity with the option of including rate effects. It is a very cost-effective model and is available for shell, solid, and beam elements. Gao [21, 22] and Tan et al. [23] also used the bilinear strain-hardening material model in their research studies.

The structure of CHCs is shown in Figure 2(a). The cell structural parameters of CHCs are side length (l), width (h), wall thickness (t), expansion angle (q), depth (b), edge length ratio (h/l), and the ratio of cell wall thickness to edge length (t/l). l of all specimen is equal to 3 mm. b of all specimen is equal to 10 mm. The other parameters were divided into two groups. The first group was used to study the influence of different wall thickness on the in-plane cushioning performance of CHCs. The second group is used to study the influence of different expansion angles on the in-plane cushioning performance of CHCs. The specific parameters are shown in Tables 3 and 4.

2.2. Model Verification. In order to ensure the reliability of the model, the present FE model is shown in Figure 1, which is similar to the models used by Ruan et al. used by Ruan et al. [24], Zheng et al. [25], Li et al. [26], Ali et al. [27], Liu and Zhang [28], and Sun and Zhang [20].

In addition, to verify the accuracy and reliability of the finite element algorithm and model, the in-plane dynamic mechanical properties of a hexagonal honeycomb structure are simulated using the loading conditions described in Reference [19], where all degrees of freedom are constrained on the bottom side of the specimen, while the other edges are free in plane. The impact plate collides with the specimen at a constant speed. As shown in Figure 3, the simulation results are basically consistent with the research results in Reference [19] and can effectively reproduce the formation of "W" deformation bands in the dynamic impact process of concave hexagonal honeycomb structures, which proves the reliability of the modeling and algorithm in this paper.

Table 1: Crushing velocity parameters.

Velocity	Specific value (m/s)							
v	3	20	50	70	100	150	200	250

3. Dynamic Cushioning Coefficient

According to the cushioning performance analysis theory, the cushioning coefficient is the ratio of the applied force to the deformation energy per unit thickness. The cushioning coefficient curve can be used to characterize the cushioning properties of materials, which can consider many factors such as the force area and thickness. The dynamic cushioning coefficient can reflect the energy absorption properties of materials in practical applications more accurately and truly, and it can overcome the deficiency of statics parameters characterization. It is of great reference significance for the application and optimization design of CHCs.

3.1. Optimal Unit Volume Energy Absorption Point. According to the "cushioning coefficient-maximum stress curve" method, the cushioning coefficient can be calculated by the following three formulas:

$$C = \frac{\sigma}{e}, \tag{1}$$

$$\sigma = \frac{F}{A}, \tag{2}$$

$$e = \int_0^{\varepsilon} \sigma \mathrm{d}\varepsilon, \tag{3}$$

where C is the cushioning coefficient, dimensionless. e is the energy absorption per unit volume of the buffer material (g/cm^2). ε is strain, and F is the force (KN). A is the bearing area of the sample (cm^2).

The force and displacement curves $F-u$ of CHCs obtained by the finite element method are shown in Figure 4. According to the characteristics of the curve, it was first simplified to get the simplified curve as shown in Figure 5 and then standardized to get the corresponding stress-strain curve. Obviously, the obtained stress-strain curve is also a four stage.

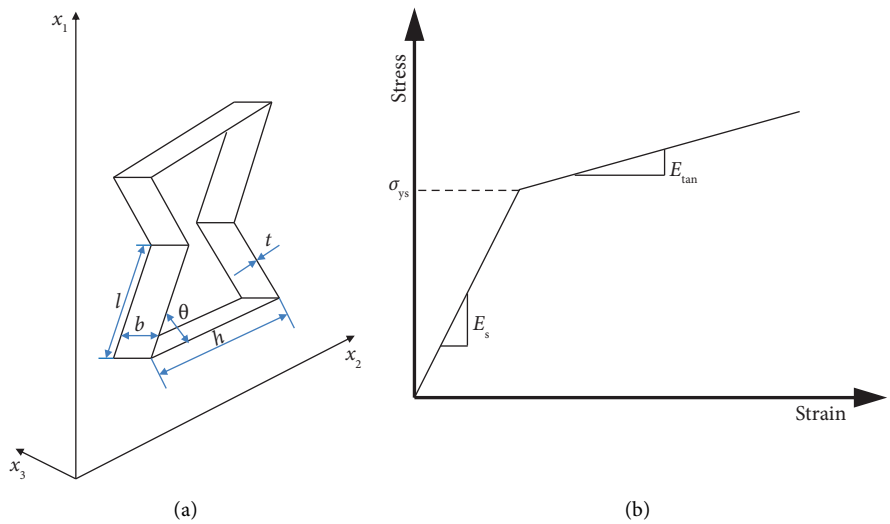

Figure 2: Configuration of concave hexagonal honeycomb cores. (a) Cell structure parameters. (b) Stress-strain curve for bilinear plastic cell wall material.

Table 2: Matrix material parameters.

Matrix material	Poisson's ratio	Yield stress (MPa)	Tangent modulus (MPa)	Young modulus (GPa)	Density (kg/m^3)
Al	0.35	292	689.7	68.97	2700

Table 3: The first group of configuration parameters.

θ(°) and h/l	t (mm)							
$\theta = 30°$, $h/l = 2.0$	0.02	0.05	0.08	0.10	0.15	0.20	0.25	0.30
$\theta = 45°$, $h/l = 2.5$	0.02	0.05	0.08	0.10	0.15	0.20	0.25	0.30
$\theta = 60°$, $h/l = 1.5$	0.02	0.05	0.08	0.10	0.15	0.20	0.25	0.30

Table 4: The second group of configuration parameters.

t (mm) and h/l	θ(°)							
$t = 0.05$ mm, $h/l = 2.0$	10	20	30	40	50	60	70	80
$t = 0.10$ mm, $h/l = 2.5$	10	20	30	40	50	60	70	80
$t = 0.20$ mm, $h/l = 3.0$	10	20	30	40	50	60	70	80

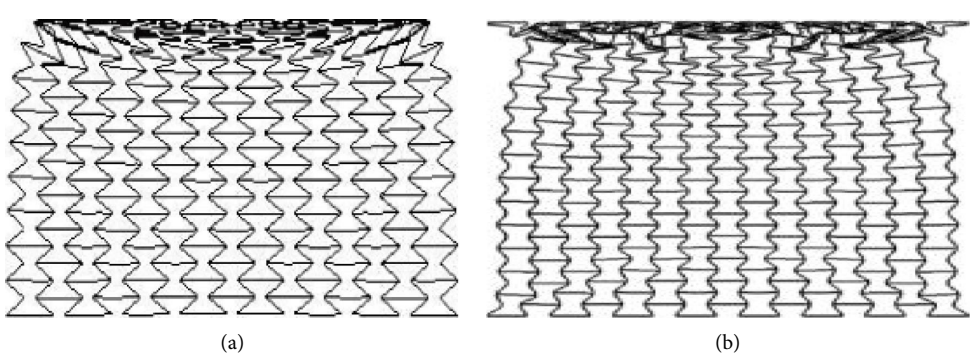

Figure 3: In-plane impact deformation modes of concave hexagonal honeycomb cores. (a) This paper. (b) Reference [19].

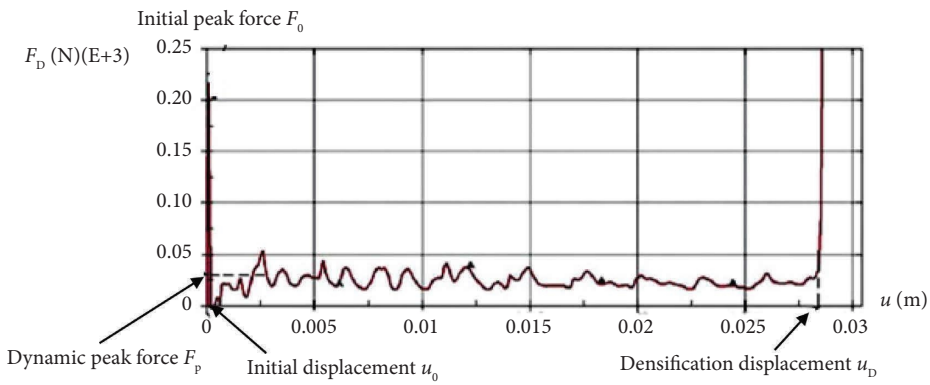

Figure 4: $F-u$ curve ($t=0.10$ mm, $h/l=2.5$, $v=100$ m/s, and $\theta=30^\circ$).

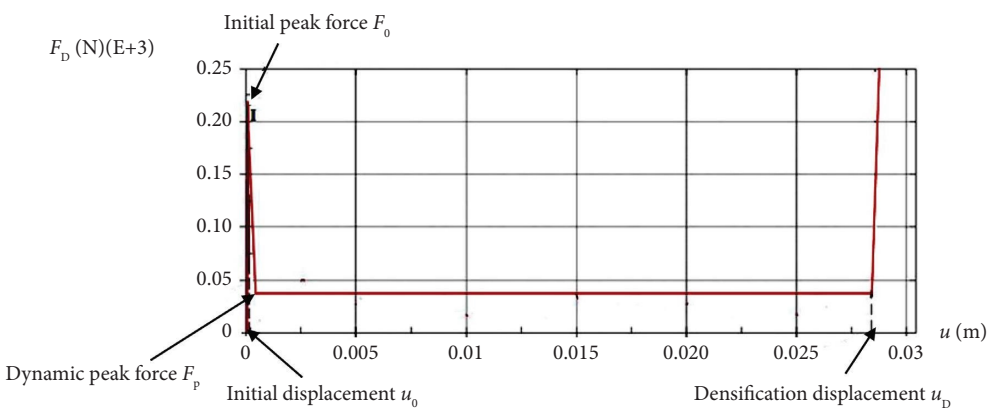

Figure 5: Simplified $F-u$ curve ($t=0.10$ mm, $h/l=2.5$, $v=100$ m/s, and $\theta=30^\circ$).

The stress solving equation of CHCs corresponding to four stages is as follows:

$$\begin{cases} \sigma = E_d\varepsilon, & 0 \le \varepsilon < \varepsilon_0, \\ \sigma_p \le \sigma \le \sigma_0 & \varepsilon = \varepsilon_0, \\ \sigma = \sigma_p, & \varepsilon_0 < \varepsilon \le \varepsilon_D, \\ \sigma = \sigma_p + E_s(\varepsilon - \varepsilon_D), & \varepsilon_D < \varepsilon < 1. \end{cases} \tag{4}$$

The corresponding simplified four-section $e-\varepsilon$ curve is as follows:

$$\begin{cases} e = \dfrac{E_d\varepsilon^2}{2}, & 0 \le \varepsilon < \varepsilon_0, \\ e = \dfrac{E_d\varepsilon_0^2}{2}, & \varepsilon = \varepsilon_0, \\ e = \dfrac{E_d\varepsilon_0^2}{2} + \sigma_p(\varepsilon - \varepsilon_0), & \varepsilon_0 < \varepsilon \le \varepsilon_D, \\ e = \dfrac{E_d\varepsilon_0^2}{2} + \sigma_p(\varepsilon_D - \varepsilon_0) + \dfrac{E_s(\varepsilon - \varepsilon_0)^2}{2}, & \varepsilon_D < \varepsilon < 1. \end{cases} \tag{5}$$

Define dynamic cushioning coefficient $C=\sigma/e$. Therefore, the simplified "dynamic cushioning coefficient-strain" relationship model is as follows:

$$\begin{cases} C = \dfrac{2}{\varepsilon}, & 0 \le \varepsilon < \varepsilon_0, \\ \dfrac{2}{\varepsilon_0} \le C \le \dfrac{(2\sigma_p)}{(E_d\varepsilon_0^2)}, & \varepsilon = \varepsilon_0, \\ C = \dfrac{\sigma_p}{\left[{\sigma_0}^2/(2E_d) + \sigma_p(\varepsilon - \varepsilon_0)\right]}, & \varepsilon_0 < \varepsilon \le \varepsilon_D, \\ C = \dfrac{\left[\sigma_p + E_s(\varepsilon - \varepsilon_D)\right]}{\left[E_d\varepsilon_0^2/2 + \sigma_p(\varepsilon_D - \varepsilon_0) + E_s(\varepsilon - \varepsilon_D)^2/2\right]}, & \varepsilon_D < \varepsilon < 1. \end{cases} \tag{6}$$

The typical "dynamic cushioning coefficient-strain" curve of CHCs can be obtained by MATLAB programming, as shown in Figure 6.

According to the abovementioned method, dynamic cushioning coefficient-strain curves of all samples can be obtained, and their morphology is similar to that of Figure 6. There is a minimum point on each dynamic cushioning

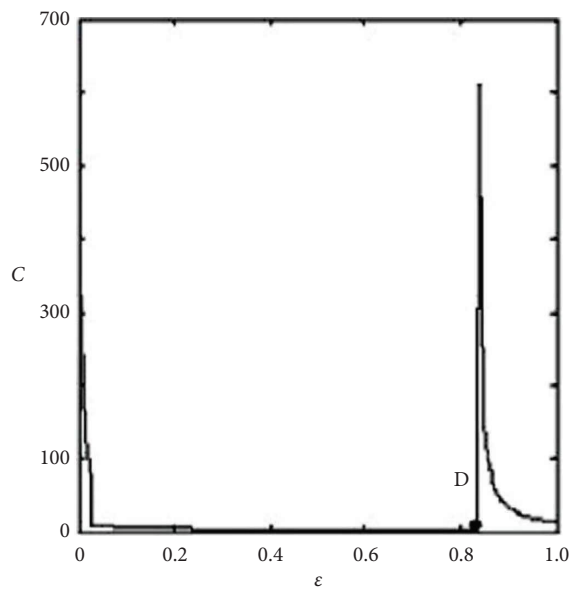

Figure 6: Typical curve of $C - \varepsilon$ ($t = 0.10$ mm, $h/l = 2.5$, $v = 100$ m/s, and $\theta = 30°$).

coefficient-strain curve, corresponding to point D in Figure 6. Here, the ordinate corresponding to point D is defined as the minimum dynamic cushioning coefficient C_D, and the corresponding abscissa is the abovementioned densification strain D and the corresponding energy absorption value e_D is defined as "the optimal energy absorption point per unit volume."

The quantity absorption value e_D is defined as "optimal unit volume energy absorption." Therefore, the point D is called the "optimal unit volume energy absorption point." The smaller the minimum dynamic buffer coefficient value, the higher the energy absorption efficiency of the material, that is, the better the cushioning performance of the material. Therefore, the point D is called the "optimal unit volume energy absorption point." The smaller the minimum dynamic cushioning coefficient value, the higher the energy absorption efficiency of the material, that is, the better the cushioning performance of the material.

3.2. The Value of Minimum Dynamic Cushioning Coefficient (MDCC). As mentioned above, the density energy absorption value can be obtained by FEM, and then divided by the volume of the sample, the density energy absorption per unit volume can be calculated, that is, the optimal energy absorption per unit volume e_D. The MDCC can be calculated by the following formula.

As mentioned above, the densified energy absorption value can be obtained by FEM. The densified energy absorption per unit volume, i.e., the optimal energy absorption per unit volume e_D, is equal to the densified energy absorption value divided by the volume of the sample. The value of MDCC can be calculated by the following formula.

$$C_D = \frac{\sigma_p}{e_D}. \tag{7}$$

Based on FEM calculation results, the calculated value of MDCC of each sample are listed in Tables 5–10. It can be seen from the table that the values of MDCC are greater than and close to 1, which can be theoretically explained from the following analysis. According to equation (5), the value of e_D for optimal unit volume energy absorption is shown in the following.

$$e_D = \frac{E_d \varepsilon_0^2}{2} + \sigma_p (\varepsilon_D - \varepsilon_0). \tag{8}$$

The stress corresponding to e_D is the average stress in the platform area, namely, the dynamic peak stress σ_p, which corresponds to the MDCC. As can be seen from the impact force-displacement curve of CHCs (see Figure 4), the initial displacement in the linear elastic stage is very small, and the corresponding energy absorption is very small. ε_0 is approximately equal to 0, so the formula of MDCC is as follows:

$$e_D \approx \sigma_p \varepsilon_D, \tag{9}$$

$$C_D \approx \frac{1}{\varepsilon_D}. \tag{10}$$

Theoretically, the value of MDCC can be approximated as the reciprocal of the densification strain. Also, since e_D is less than 1, the value of MDCC are all greater than 1. According to the results of numerical analysis, e_D ranges from 0.70 to 0.95 and tends to 1 with the increase of impact velocity. Therefore, the value of MDCC is going to be close to 1.

4. Analysis of Results

4.1. Influence of the Expansion Angle on MDCC. Under different impact loads, when other structural parameters are fixed, the MDCC value of CHCs with different expansion angles are listed in Tables 5–7 and Figures 7–9. The results show that the value of MDCC decreases with the increase of the expansion angle at the same impact velocity.

The relative density of honeycomb core material [29, 30] is

$$\overline{\rho} = \left(2h + 4l - \frac{2t}{\sin\theta} - \frac{t}{\tan\theta}\right) \times \left\{\frac{1}{[4(h - l \times \cos\theta)\sin\theta]}\right\} \times \left(\frac{t}{l}\right). \tag{11}$$

Table 5: C_D for different at different v ($h/l = 2.0$ and $t = 0.05$ mm).

v (m/s)	θ (°)							
	10	20	30	40	50	60	70	80
3	1.3513	1.1834	1.1604	1.1586	1.1568	1.1485	1.1423	1.1301
20	1.257	1.1542	1.1491	1.1484	1.1435	1.1308	1.1307	1.1244
50	1.2501	1.1401	1.1395	1.1373	1.1358	1.1285	1.1228	1.1206
70	1.2249	1.1107	1.1339	1.1326	1.1333	1.1137	1.1101	1.1007
100	1.239	1.1076	1.1308	1.13	1.1177	1.0782	1.0692	1.0568
150	1.2389	1.1063	1.128	1.0999	1.077	1.0589	1.0501	1.0409
200	1.2332	1.105	1.0833	1.081	1.0695	1.0619	1.0494	1.0435
250	1.2302	1.1004	1.073	1.0708	1.0586	1.0553	1.0464	1.0366

Table 6: C_D for different θ at different v ($h/l = 2.5$ and $t = 0.1$ mm).

v (m/s)	θ (°)							
	10	20	30	40	50	60	70	80
3	1.7805	1.3867	1.241	1.221	1.2091	1.2066	1.2043	1.1234
20	1.6184	1.3156	1.2052	1.1845	1.1824	1.1903	1.2123	1.1659
50	1.5789	1.2714	1.174	1.1743	1.1657	1.1886	1.1924	1.1912
70	1.6045	1.2553	1.1535	1.1554	1.1663	1.0959	1.1397	1.0962
100	1.5933	1.2969	1.1793	1.1526	1.1568	1.1107	1.1111	1.0731
150	1.5526	1.2443	1.1594	1.1512	1.1234	1.0895	1.0835	1.0435
200	1.5597	1.2335	1.1559	1.1362	1.0985	1.0796	1.0593	1.0247
250	1.5306	1.2388	1.1249	1.1247	1.092	1.0797	1.0607	1.0095

Table 7: C_D for different θ at different v ($h/l = 3.0$ and $t = 0.2$ mm).

v (m/s)	θ (°)							
	10	20	30	40	50	60	70	80
3	1.9246	1.4021	1.2611	1.3659	1.3303	1.3029	1.2996	1.2723
20	1.8357	1.3798	1.2375	1.2417	1.2466	1.2521	1.2414	1.2546
50	1.7747	1.3026	1.2116	1.2151	1.2299	1.2398	1.2356	1.2279
70	1.7491	1.3073	1.1958	1.2764	1.216	1.1809	1.1122	1.1072
100	1.6867	1.2859	1.1826	1.1649	1.1922	1.1745	1.1245	1.1258
150	1.6782	1.2622	1.1734	1.1341	1.1858	1.1654	1.1055	1.1255
200	1.6878	1.272	1.1669	1.1241	1.1922	1.1432	1.1222	1.1109
250	1.6652	1.2588	1.1804	1.123	1.1158	1.1098	1.071	1.054

Table 8: C_D for different t at different v ($l = 3$ mm, $h/l = 1.5$, and $\theta = 60°$).

v (m/s)	t (mm)							
	0.02	0.05	0.08	0.1	0.15	0.2	0.25	0.3
3	1.193	1.378	1.4751	1.4949	1.4964	1.5002	1.5349	1.5802
20	1.1058	1.2089	1.3623	1.3463	1.3555	1.3798	1.382	1.3936
50	1.1241	1.2001	1.3365	1.3438	1.3343	1.3492	1.3522	1.3842
70	1.0722	1.1649	1.2317	1.2447	1.2554	1.2934	1.2987	1.3166
100	1.0618	1.106	1.1594	1.1945	1.2488	1.2814	1.2918	1.2929
150	1.0596	1.0738	1.1135	1.1486	1.1882	1.196	1.2247	1.2523
200	1.0625	1.0549	1.081	1.106	1.1226	1.1348	1.1492	1.1566
250	1.0537	1.0618	1.0748	1.0845	1.1117	1.1104	1.1053	1.1109

When other structural parameters are fixed and the expansion angle varies from 10° to 80°, the relation curve between the relative density and the expansion angle of the CHCs can be obtained according to equation (11), as shown in Figure 10. The results show that with the increase of the expansion angle, the relative density gradually decreases and the attenuation decreases. When the expansion angle reaches about 80°, the relative density hardly decreases. At a given impact velocity, the densification strain tends to increase with the decrease of relative density. It can also be seen from equation (10) that the value of MDCC is approximately inversely proportional to the densification

Table 9: C_D for different t at different v ($l = 3$ mm, $h/l = 2.5$, and $\theta = 45°$).

v (m/s)	t (mm)							
	0.02	0.05	0.08	0.1	0.15	0.2	0.25	0.3
3	1.129	1.1444	1.1881	1.213	1.2132	1.2186	1.21946	1.2206
20	1.1118	1.1288	1.1541	1.1672	1.169	1.1711	1.173	1.1743
50	1.0982	1.1112	1.1471	1.162	1.1659	1.167	1.1711	1.1723
70	1.0701	1.1107	1.1439	1.1527	1.1547	1.1466	1.1569	1.1616
100	1.0769	1.1031	1.1353	1.1491	1.1501	1.145	1.1463	1.1547
150	1.0773	1.0749	1.1043	1.1345	1.1405	1.1424	1.1492	1.1544
200	1.067	1.0733	1.0877	1.1051	1.1305	1.1321	1.1309	1.1326
250	1.0612	1.07	1.0824	1.094	1.1154	1.1121	1.1105	1.1115

Table 10: C_D for different t at different v ($l = 3$ mm, $h/l = 2.0$, and $\theta = 30°$).

v (m/s)	t (mm)							
	0.02	0.05	0.08	0.1	0.15	0.2	0.25	0.3
3	1.1839	1.1894	1.1959	1.2071	1.2231	1.2484	1.2541	1.2896
20	1.1696	1.166	1.1762	1.1938	1.2189	1.2389	1.2449	1.2744
50	1.165	1.1637	1.1713	1.1796	1.2124	1.2237	1.2202	1.2268
70	1.1333	1.1353	1.1417	1.1692	1.1989	1.2087	1.2144	1.2214
100	1.098	1.098	1.1394	1.1645	1.193	1.2031	1.2103	1.221
150	1.0909	1.0879	1.1322	1.1639	1.1794	1.1836	1.1843	1.1878
200	1.0644	1.0676	1.1177	1.1525	1.1757	1.173	1.174	1.1772
250	1.0502	1.0533	1.1014	1.1404	1.1516	1.1587	1.1609	1.1651

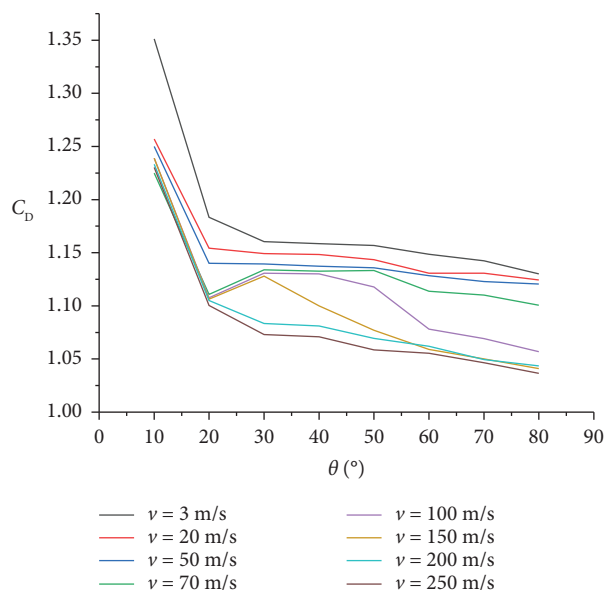

Figure 7: C_D for different at different v ($h/l = 2.0$ and $t = 0.05$ mm).

strain. Therefore, at a given impact velocity, when other structural parameters are constant, the value of MDCC of CHCs will decrease with the increase of the expansion angle. This is also proved by the calculation results in Tables 5–7.

4.2. Influence of Cell Wall Thickness to Edge Length (t/l Ratio) on MDCC. At different impact velocities and when other structural parameters are constant, the value of MDCC of CHCs with different t/l ratio is listed in Tables 8–10, corresponding to Figures 11–13. It shows that the value of MDCC increases with the increase of the t/l ratio at the same impact velocity.

According to equation (11), the relation curve between the relative density and t/l ratio of CHCs is shown in Figure 14. As can be seen from the figure, when other structural parameters are constant, the relative density increases with the increase of the t/l ratio, and the densification strain

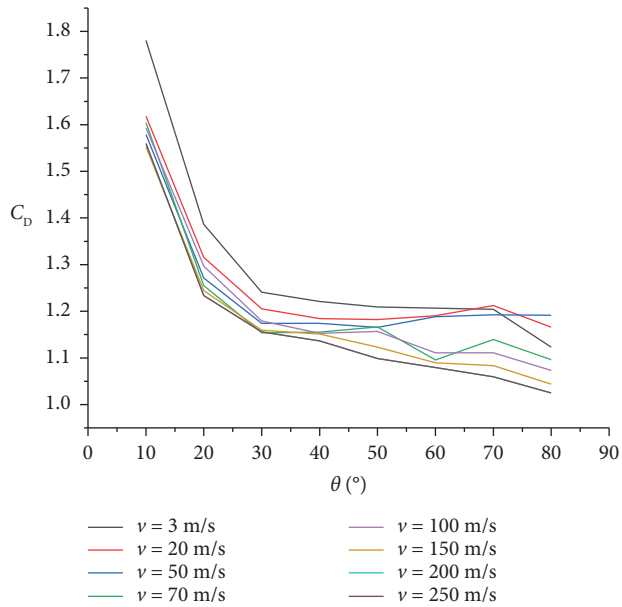

Figure 8: C_D for different θ at different v ($h/l = 2.5$ and $t = 0.1$ mm).

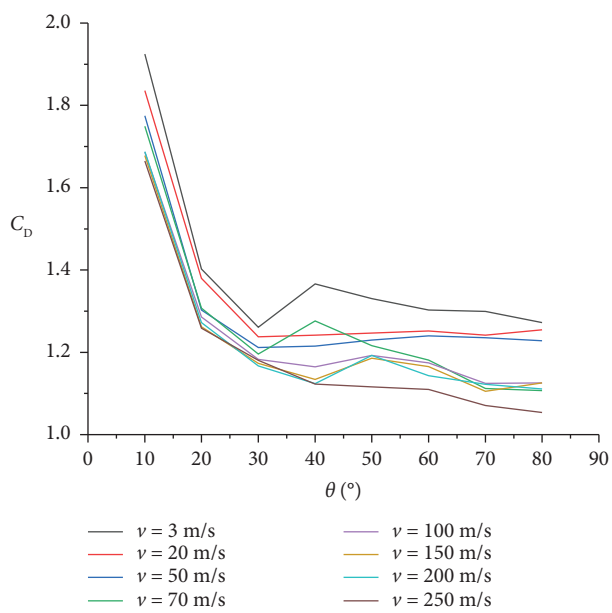

Figure 9: C_D for different θ at different v ($h/l = 3.0$ and $t = 0.2$ mm).

decreases with the increase of relative density. According to the analysis theory of the simplified model, the relationship between MDCC and densification strain is approximately inversely proportional. Therefore, under a given impact velocity load, the value of MDCC will increase with the increase of the t/l ratio. This is also proved by the calculation results in Tables 8–10.

4.3. Influence of Impact Velocity on Cushioning Performance and Deformation Modes. From Tables 5 to 10, it can be seen that when all structural parameters are constant, the value of MDCC of CHCs decreases with the increase of impact velocity. This physical phenomenon can be explained by the deformation modes of CHCs under different impact velocities.

The deformation modes of CHCs are obtained by simulation calculation under low speed, medium speed, and high impact load, as shown in Figures 15–17. For the quasistatic deformation mode at low speed (Figure 15), the deformation mode of each part of CHCs is uniform, and the densification of all parts occurs almost simultaneously. At the first stage, a local collapse zone in the shape of "W" first appears near the pressure plate. When the deformation of

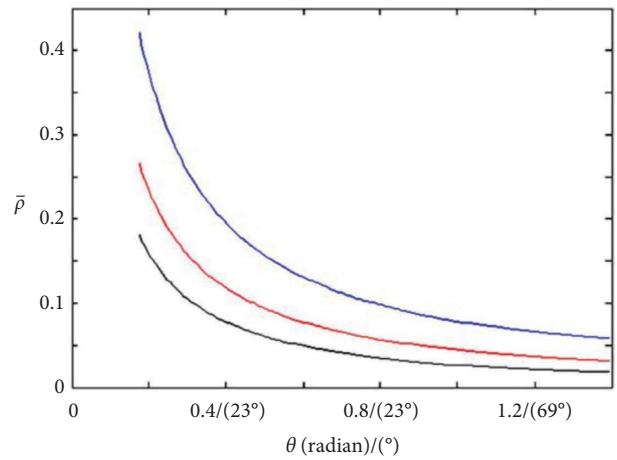

Figure 10: $\bar{\rho} - \theta$ curve of CHCs with fixed l, h/l, and t.

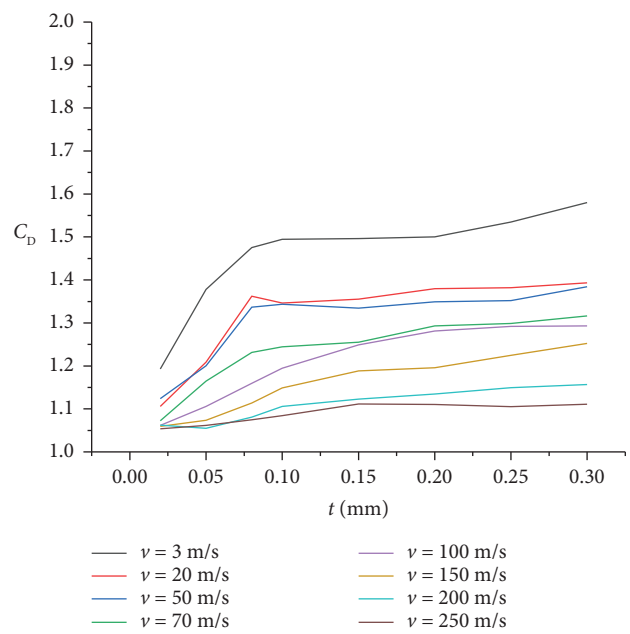

Figure 11: C_D for different t at different v ($l = 3$ mm, $h/l = 1.5$, and $\theta = 60^\circ$).

CHCs is less than 20%, it can be clearly seen that "M"-shaped deformation zone appears at the support plate, and with the further deepening of the impact end, "W" collapse zone, the shape of "double W". When the deformation propagates to some extent, the cells in the center of the specimen begin deformation appearing in the indistinct "X"-shaped form with extension deformation on both sides (see Figure 15(d)). All collapse bands evolve gradually until the top and bottom local deformation bands touch and are absolutely crushed to densification (see Figures 15(e) and 15(f)).

Under the medium-speed impact (see Figure 16), the collapse zone of CHCs slowly begins to converge towards the upward direction of the pressure plate, accompanied by the collapse of the lower part. Such a deformation mode also determines that with the increase of impact velocity, the strain at the arrival of densification will be gradually larger. In this stage, most deformation stages of CHCs will produce a "W"-shaped deformation belt near the pressure plate, and only in the later stage, a cross-sloping deformation belt can be produced.

Under the high-speed impact (see Figure 17), the deformation of CHCs only occurs near the upper pressure plate, in the shape of "–". No inclined deformation belt is generated in the whole process. When the upper pressure plate is almost completely close to the lower support plate, the whole material will enter the densification stage. It can also be seen that when the deformation mode of "–" occurs, the densification strain of the sample will increase to a certain value and will not change with the further increase of impact velocity.

According to the above analysis, when the structural parameters are constant, before the dynamic deformation mode occurs, the densification strain of CHCs also increases with the increase of impact velocity. According to formula

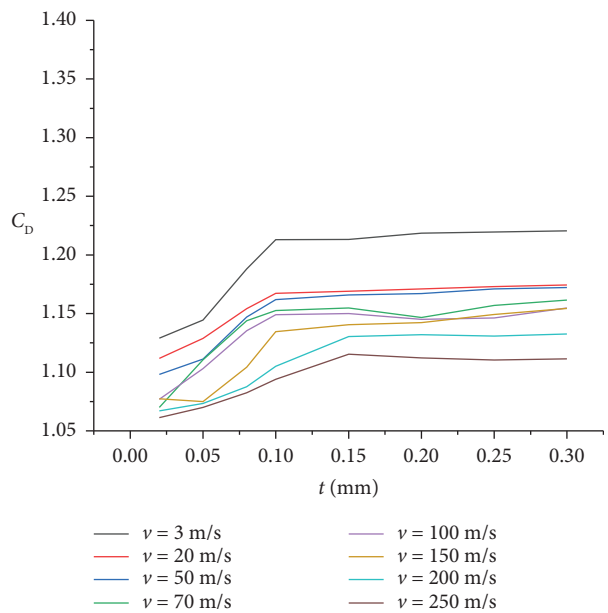

Figure 12: C_D for different t at different v ($l = 3$ mm, $h/l = 2.5$, and $\theta = 45^\circ$).

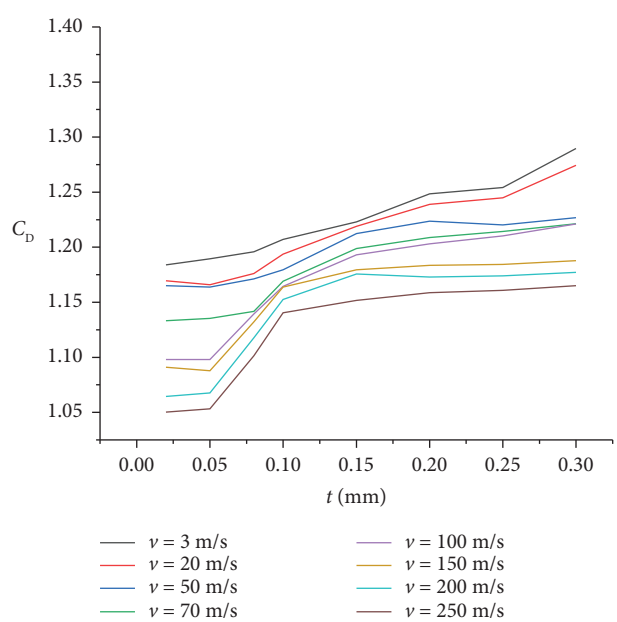

Figure 13: C_D for different t at different v ($l = 3$ mm, $h/l = 2.0$, and $\theta = 30^\circ$).

(12), under the premise of fixed structural parameters, the value of MDCC of CHCs decreases with the increase of impact velocity.

When $t = 0.05$ mm and $h/l = 2$, the deformation modes of CHCs with different expansion angles under different impact velocity loads are shown in Figure 18(a). It can be found that when the expansion angle increases from 10° to 80°, the critical conversion velocity between deformation modes hardly depends on the expansion angle. When $h/l = 2$ and $\theta = 30^\circ$, the deformation modes of CHCs with different wall thickness and side length ratios under different impact velocity loads are shown in Figure 18(b). The critical velocity v_1 of the transformation from "M" to "W" is almost independent of the wall thickness and side length ratio, and it is shown as a horizontal straight line. The critical velocity v_2 of the transition from "W" to "one" is related to the wall thickness side length ratio.

As $\sigma \propto (t/l)^2$, $\rho \propto t/l$ [31], the critical deformation mode conversion velocity is $v \propto (t/l)^{1/2}$, and it can be obtained by [32]. When $h/l = 2$ and $\theta = 30^\circ$, based on the finite element numerical analysis results, the empirical formula of the change of the critical transformation velocity of the deformation mode with the wall thickness side length ratio can be obtained by the least square method as follows:

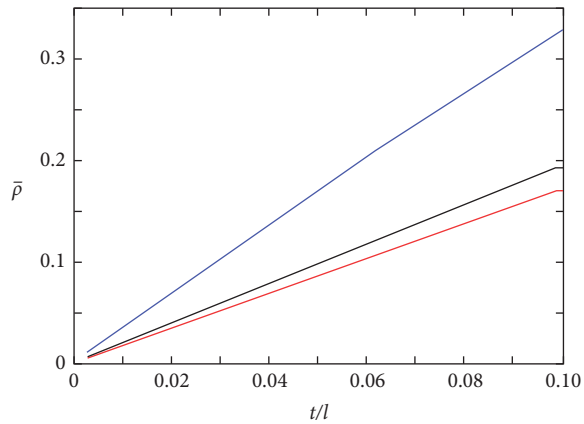

Figure 14: $\bar{\rho} - t/l$ curve of the concave hexagonal honeycomb cores with fixed h/l and θ.

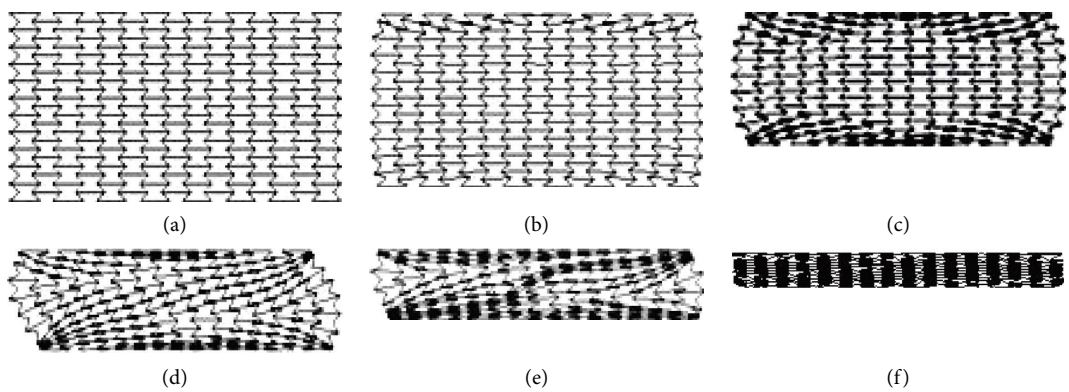

Figure 15: Deformation stages of CHCs ($v = 3$ m/s, $l = 3$ mm, $t = 0.05$ mm, $h/l = 2.5$, and $\theta = 45^\circ$). (a) $T = 0.9965$ ms. (b) $T = 1.7653$ ms. (c) $T = 4.7710$ ms. (d) $T = 8.110$ ms. (e) $T = 10.496$ ms. (f) $T = 13.3590$ ms.

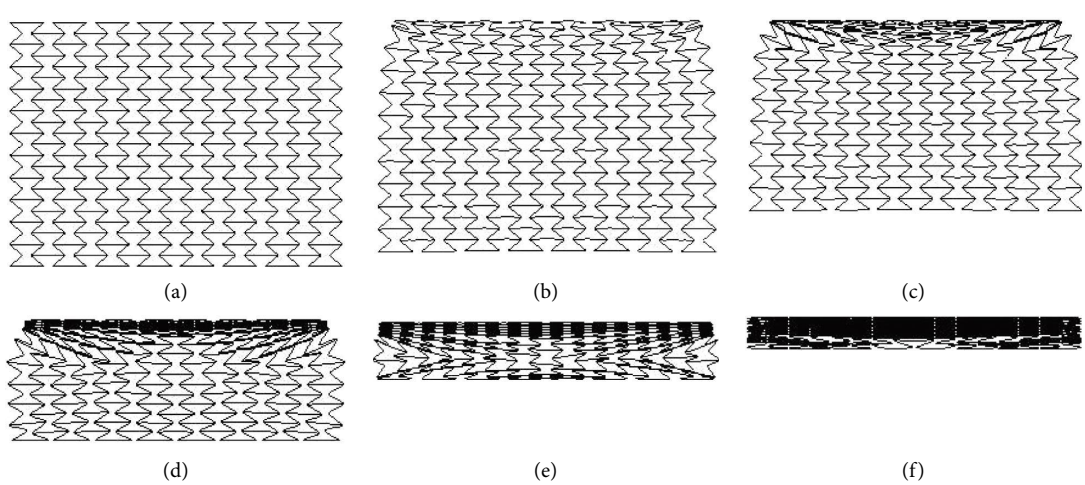

Figure 16: Deformation stages of CHCs ($v = 20$ m/s, $l = 3$ mm, $t = 0.05$ mm, $h/l = 2.5$, and $\theta = 45^\circ$). (a) $T = 0$ ms. (b) $T = 0.16258$ ms. (c) $T = 0.4943$ ms. (d) $T = 1.1579$ ms. (e) $T = 1.5872$ ms. (f) $T = 1.906$ ms.

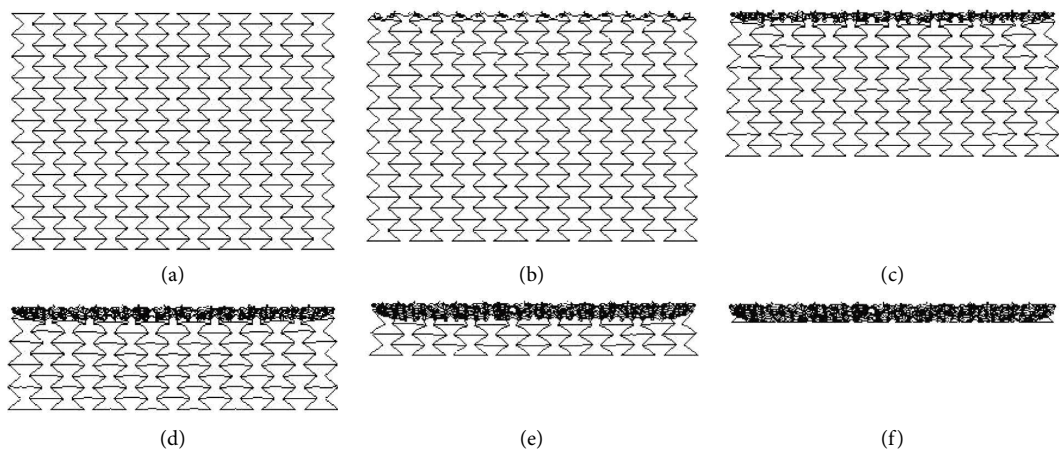

Figure 17: Deformation stages of CHCs ($v = 200$ m/s, $l = 3$ mm, $t = 0.05$ mm, $h/l = 2.5$, and $\theta = 45^\circ$). (a) $T = 0$ ms. (b) $T = 0.012683$ ms. (c) $T = 0.081976$ ms. (d) $T = 0.12557$ ms. (e) $T = 0.16427$ ms. (f) $T = 0.19210$ ms.

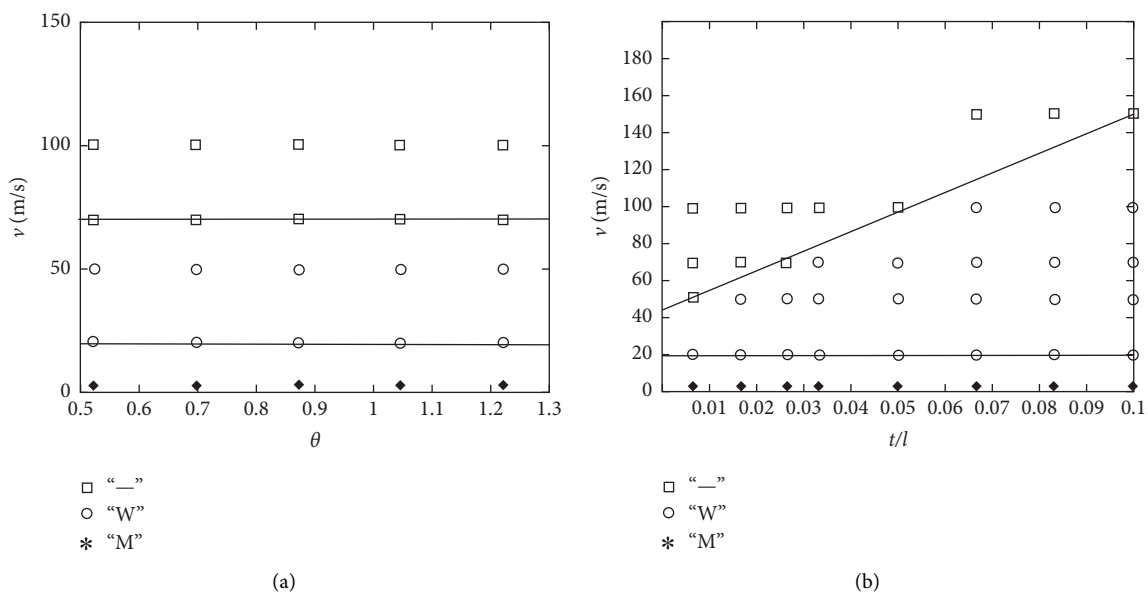

Figure 18: (a) Deformation mode map with different at different impact velocities ($t = 0.05$ mm and $h/l = 2$) and (b) deformation mode map with different cell wall thicknesses at different impact velocities ($h/l = 2$ and $\theta = 30^\circ$).

$$v_1 = 20\,(\mathrm{m/s}), \tag{12}$$

$$v_2 \approx 425\left(\frac{t}{l}\right)^{1/2}\,(\mathrm{m/s}). \tag{13}$$

5. Conclusion

In this paper, the dynamic cushioning coefficient is used to characterize the cushioning performance of CHCs. According to the characteristics of dynamic stress-strain curves, a simplified energy absorption model was proposed. Based on the simplified mode, the value of MDCC of CHCs is obtained to characterize the cushioning performance. It is a methodological innovation.

The influence of structural parameters and impact velocity on the MDCC is analyzed. When the structural parameters are constant, the MDCC of CHCs decreases with the increase of the impact velocity, that is, the greater the impact velocity, the higher the energy absorption efficiency of CHCs and the better the cushioning performance. When the impact velocity and other parameters are constant, the MDCC of CHCs increases with the increase of the wall thickness side length ratio and decreases with the increase of the expansion angle, that is, the greater the wall thickness side length ratio, the worse the cushioning performance of CHCs, and the greater the expansion angle, the better the cushioning performance of CHCs.

It is concluded that the deformation modes of CHCs under dynamic impact load can be divided into three types. The first type is "M"-type collapse at low speed impact, the

second type is "*W*"-type transition deformation mode, and the third type is the "I-shaped" deformation mode during high-speed impact. According to the finite element simulation results, the transformation velocity of deformation mode is obtained, and the empirical expression between the transformation velocity and the structural parameters of honeycomb element is obtained.

The abovementioned conclusions are based on numerical and theoretical research fields, but it still provides guidance and basis for the practical engineering application of CHC in the future. In practical applications, the dynamic impact load may also be from out-plane direction, the matrix materials are also diverse, and the actual production process may cause some structural defects. Therefore, in the future research, the impact of different plane impact loads on the cushioning performance of CHCs can be carried out, the effects of different matrix materials on the cushioning properties of CHCs can be compared and summarized, and the influence of structural defects on the cushioning properties of CHCs can be analyzed. These studies have important guiding significance for the safe and reasonable use of CHCs.

Data Availability

The data used to support the findings of this study are included within the article.

Conflicts of Interest

The authors declare that they have no conflicts of interest.

Authors' Contributions

The authorship contributions statement of manuscript (9978340) titled "In-plane dynamic cushioning performance of Concave Hexagonal Honeycomb Cores" is as follows. We confirm that all authors meet the ICMJE criteria. No further changes to authorship will be possible after this point. Miao Liu make important contributions to the concept, thinking, topic selection, design, implementation and data acquisition, analysis of research work, writing the paper, and modifying its key contents. Yan Cao provided the research direction of the paper, solved the problems encountered, and guided the whole research process. De-Qiang Sun provided simulation ideas, solved problems encountered in simulation analysis, and adjusted and advised on the overall direction of the study. Chao-Rui Nie collated documents and participated in writing papers. Zhi-Jie Wang performed index detection, collation, and analysis of original results.

Acknowledgments

This work was supported by the National Natural Science Foundation of China (52275508), the National Natural Science Foundation of China (51575327), the Key Laboratory and Base Project of the Shaanxi Provincial Department of Education (16JS014), and the Shaanxi Provincial Department of Education 2014 Shaanxi Undergraduate University Major Comprehensive Reform Pilot Project (SJG (2014) No. 16).

References

[1] Y. F. Guo, X. X. Han, X. N. Wang, Y. G. Fu, and R. H. Xia, "Static cushioning energy absorption of paper composite sandwich structures with corrugation and honeycomb cores," *Journal of Sandwich Structures and Materials*, vol. 23, no. 4, pp. 1347–1365, 2021.

[2] M. Toyoda, K. Sakagami, D. Takahashi, and M. Morimoto, "Effect of a honeycomb on the sound absorption characteristics of panel-type absorbers," *Applied Acoustics*, vol. 72, no. 12, pp. 943–948, 2011.

[3] J. Li, X. Z. Cui, H. Qi et al., "Laboratory tests on engineering properties of a new negative-Poisson's-ratio geobelt," *Construction and Building Materials*, vol. 297, Article ID 123819, 2021.

[4] P. Mardling, A. Alderson, N. Jordan-Mahy, and C. L. Le Maitre, "The use of auxetic materials in tissue engineering," *Biomaterials Science*, vol. 8, no. 8, pp. 2074–2083, 2020.

[5] P. R. Budarapu, S. S. Yb, and R. Natarajan, "Design concepts of an aircraft wing: composite and morphing airfoil with auxetic structures," *Frontiers of Structural and Civil Engineering*, vol. 10, no. 4, pp. 394–408, 2016.

[6] K. Alderson, A. Alderson, S. Anand et al., "Auxetic warp knit textile structures," *Physica Status Solidi (B)*, vol. 249, no. 7, pp. 1322–1329, 2012.

[7] K. Pan, J. Y. Ding, W. Zhang, and S. D. Zhao, "The negative Poisson's ratio ship base design and vibration isolation performance analysis," *Applied Sciences*, vol. 11, no. 23, pp. 11167–111167, 2021.

[8] D. Li, R. C. Gao, L. Dong, W. K. Lam, and F. P. Zhang, "A novel 3D re-entrant unit cell structure with negative Poisson's ratio and tunable stiffness," *Smart Materials and Structures*, vol. 29, no. 4, Article ID 045015, 2020.

[9] T. T. Li, Y. Y. Chen, X. Y. Hu, Y. B. Li, and L. F. Wang, "Exploiting negative Poisson's ratio to design 3D-printed composites with enhanced mechanical properties," *Materials and Design*, vol. 142, pp. 247–258, 2018.

[10] C. J. Shen, T. X. Yu, and G. Lu, "Double shock mode in graded cellular rod under impact," *International Journal of Solids and Structures*, vol. 50, no. 1, pp. 217–233, 2013.

[11] C. J. Shen, G. Lu, and T. X. Yu, "Dynamic behavior of graded honeycombs- A finite element study," *Composite Structures*, vol. 98, pp. 282–293, 2013.

[12] P. W. Zhang, Z. H. Wang, and L. M. Zhao, "Dynamic crushing behavior of open-cell aluminum foam withnegative Poisson's ratio," *Applied Physics A*, vol. 123, no. 5, p. 321, 2017.

[13] Z. Y. Hu, H. Lan, and W. J. Zuo, "In-plane dynamic impact simulation of cellular materials with negative Possion's ratio," *Machinery and Electronics*, vol. 37, no. 2, pp. 31–34, 2019.

[14] F. W. Ma, H. Y. Liang, and Y. Zhao, "In-plane dynamic crushing of concave triangles materials with negative Poisson's ratio under incline load," *Journal of Vibration and Shock*, vol. 39, no. 4, pp. 81–87, 2020.

[15] G. X. Zhao, T. Fu, and J. X. Li, "Study on concave direction impact performance of similar concave hexagon honeycomb structure," *Materials*, vol. 16, no. 8, Article ID 16083262, p. 3262, 2023.

[16] A. Alomarah, S. H. Masood, and D. Ruan, "Metamaterials with enhanced mechanical properties and tuneable Poisson's ratio," *Smart Materials and Structures*, vol. 31, no. 2, pp. 025026–026, 2022.

[17] W. W. Zhang, D. Zhang, and S. S. Wang, "Review of evaluation methods for cushioning performance of energy

absorbing materials," *Packaging Engineering*, vol. 43, no. 5, pp. 143–151, 2022.

[18] D. Q. Sun, M. Liu, and Y. X. Zhu, "In-plane quasi-static crushing of cissoidal hexagonal honeycomb cores," *Advanced Materials Research*, vol. 446, pp. 3736–3739, 2012.

[19] F. G. Xu, K. J. Yu, and L. Hua, "In-plane dynamic response and multi-objective optimization of negative Poisson's ratio (NPR) honeycomb structures with sinusoidal curve," *Composite Structures*, vol. 269, no. 1, Article ID 114018, 2021.

[20] D. Q. Sun and W. H. Zhang, "Energy absorption performance of staggered triangular honeycombs under in-plane crushing loadings," *Journal of Engineering Mechanics*, vol. 139, no. 2, pp. 153–166, 2013.

[21] X. L. Gao, "An exact elasto-plastic solution for a thick-walled spherical shell of elastic linear-hardening material with finite defor-mations," *International Journal of Pressure Vessels and Piping*, vol. 57, no. 1, pp. 45–56, 1994.

[22] X. L. Gao, "Strain gradient plasticity solution for an internally pressurized thick-walled cylinder of an elastic linear-hardening material," *Zeitschrift für Angewandte Mathematik und Physik*, vol. 58, no. 1, pp. 161–173, 2007.

[23] P. J. Tan, S. R. Reid, J. J. Harrigan, Z. Zou, and S. Li, "Dynamic compressive strength properties of aluminium foams. Part II—'shock' theory and comparison with experimental data and numerical models," *Journal of the Mechanics and Physics of Solids*, vol. 53, no. 10, pp. 2206–2230, 2005.

[24] D. Ruan, G. Lu, B. Wang, and T. X. Yu, "In-plane dynamic crushing of honeycombs—a finite element study," *International Journal of Impact Engineering*, vol. 28, no. 2, pp. 161–182, 2003.

[25] Z. Zheng, J. Yu, and J. Li, "Dynamic crushing of 2D cellular structures—a finite element study," *International Journal of Impact Engineering*, vol. 32, no. 1-4, pp. 650–664, 2005.

[26] K. Li, X.-L. Gao, and J. Wang, "Dynamic crushing behavior of honeycomb structures with irregular cell shapes and non-uniform cell wall thickness," *International Journal of Solids and Structures*, vol. 44, no. 14-15, pp. 5003–5026, 2007.

[27] M. Ali, A. Qamhiyah, D. Flugrad, and M. Shakoor, "Theoretical and finite element study of a compact energy absorber," *Advances in Engineering Software*, vol. 39, no. 2, pp. 95–106, 2008.

[28] Y. Liu and X. C. Zhang, "The influence of cell micro-topology on the in-plane dynamic crushing of honeycombs," *International Journal of Impact Engineering*, vol. 36, no. 1, pp. 98–109, 2009.

[29] L. J. Gibson and M. F. Ashby, *Cellular Solids: Structures and Properties*, Cambridge University Press, Cambridge, UK, 2nd edition, 1997.

[30] X. M. Qiu, J. Zhang, and T. X. Yu, "Collapse of periodic planar lattices under uniaxial compression, part I: quasi-static strength predicted by limit analysis," *International Journal of Impact Engineering*, vol. 36, no. 10-11, pp. 1223–1230, 2009.

[31] T. L. Warren, "Negative Poisson's ratio in a transversely isotropic foam structure," *Journal of Applied Physics*, vol. 67, no. 12, pp. 7591–7594, 1990.

[32] L. J. Gibson and M. F. Ashby, "The mechanics of three-dimensional cellular materials," *Proceedings of the Royal Society of London Series A: Mathematical, Physical and Engineering Sciences*, vol. 382, pp. 43–59, 1982.